



Article

Highly Efficient Antimicrobial Activity of $\text{Cu}_x\text{Fe}_y\text{O}_z$ Nanoparticles against Important Human Pathogens

Lu Zhu ¹, David W. Pearson ², Stéphane L. Benoit ³ , Jing Xie ⁴, Jitendra Pant ¹, Yanjun Yang ¹, Arnab Mondal ¹ , Hitesh Handa ¹, Jane Y. Howe ⁵, Yen-Con Hung ⁴, Jorge E. Vidal ⁶, Robert J. Maier ³ and Yiping Zhao ^{2,*}

¹ School of Chemical, Materials and Biomedical Engineering, College of Engineering, University of Georgia, Athens, GA 30602, USA; zhulu5466@gmail.com (L.Z.); jp50261@uga.edu (J.P.); YanjunYang@uga.edu (Y.Y.); Arnab.Mondal@uga.edu (A.M.); hhanda@uga.edu (H.H.)

² Department of Physics and Astronomy, University of Georgia, Athens, GA 30602, USA; davidwpuga@gmail.com

³ Department of Microbiology, University of Georgia, Athens, GA 30602, USA; stefbens@uga.edu (S.L.B.); rmaier@uga.edu (R.J.M.)

⁴ Department of Food Science & Technology, University of Georgia, Griffin, GA 30223, USA; jing.xie25@uga.edu (J.X.); yhung@uga.edu (Y.-C.H.)

⁵ Department of Materials Science & Engineering, University of Toronto, Toronto, ON M5S 1A1, Canada; jane.howe@utoronto.ca

⁶ Department of Microbiology and Immunology, University of Mississippi, Jackson, MS 39216, USA; jvidal@umc.edu

* Correspondence: zhaoy@uga.edu

Received: 24 October 2020; Accepted: 17 November 2020; Published: 20 November 2020



Abstract: The development of innovative antimicrobial materials is crucial in thwarting infectious diseases caused by microbes, as drug-resistant pathogens are increasing in both number and capacity to detoxify the antimicrobial drugs used today. An ideal antimicrobial material should inhibit a wide variety of bacteria in a short period of time, be less or not toxic to normal cells, and the fabrication or synthesis process should be cheap and easy. We report a one-step microwave-assisted hydrothermal synthesis of mixed composite $\text{Cu}_x\text{Fe}_y\text{O}_z$ ($\text{Fe}_2\text{O}_3/\text{Cu}_2\text{O}/\text{CuO}/\text{CuFe}_2\text{O}$) nanoparticles (NPs) as an excellent antimicrobial material. The 1 mg/mL $\text{Cu}_x\text{Fe}_y\text{O}_z$ NPs with the composition 36% CuFeO_2 , 28% Cu_2O and 36% Fe_2O_3 have a general antimicrobial activity greater than 5 log reduction within 4 h against nine important human pathogenic bacteria (including drug-resistant bacteria as well as Gram-positive and Gram-negative strains). For example, they induced a >9 log reduction in *Escherichia coli* B viability after 15 min of incubation, and an ~8 log reduction in multidrug-resistant *Klebsiella pneumoniae* after 4 h incubation. Cytotoxicity tests against mouse fibroblast cells showed about 74% viability when exposed to 1 mg/mL $\text{Cu}_x\text{Fe}_y\text{O}_z$ NPs for 24 h, compared to the 20% viability for 1 mg/mL pure Cu_2O NPs synthesized by the same method. These results show that the $\text{Cu}_x\text{Fe}_y\text{O}_z$ composite NPs are a highly efficient, low-toxicity and cheap antimicrobial material that has promising potential for applications in medical and food safety.

Keywords: antimicrobial materials; inorganic nanomaterials; drug-resistant bacteria; metal oxides; copper iron oxides; copper oxide; cuprous oxide

1. Introduction

Infectious diseases are the second leading cause of death in the world (third in the United States) and the leading cause of disability-adjusted life years worldwide (1 disability-adjusted life year is one lost year of healthy life) [1–5]. Bacterial-mediated infections, including those due to *Salmonella*,

Escherichia coli, or *Shigella*, contribute to a large portion of overall infections, including, for example, the recent outbreak of *Listeria* infections linked to Deli ham [6] and *Salmonella* infections linked to ground beef [7]. Penicillin, and subsequently other antibiotics, have been critical for combating pathogens, but the increased antibiotic resistance observed in these pathogens has become an extremely serious public health concern [8]. Even when drug resistance is not the factor limiting their use, other disadvantages of antibiotics, such as their toxicity to the host, lead to the additional need to explore the efficacy of novel antimicrobial reagents [9]. New antimicrobial approaches other than the use of antibiotics have been proposed and developed, some of which include photodynamic therapy [10] and bacteria inactivation by nanoparticles [11,12]. In particular, with the advance of nanotechnology, the use of nano-sized inorganic materials as antimicrobial agents has attracted increasing attention for the control of the microbes [13–17]. The inorganic antimicrobial materials can be divided into two major categories based on their action mechanisms—the photocatalytic antimicrobial materials (activated by light), and nanomaterials that can directly lead to bacteria elimination or death (direct antimicrobial nanomaterials). Due to the advanced oxidation processes induced by photocatalytic properties, metal oxide-based photocatalytic nanomaterials have shown great promise as effective non-targeted disinfectants against a wide range of microorganisms and the decomposition of chemical contaminants [18–28]. The requirement of different wavelengths of light to activate the bactericidal activity of these materials has pros and cons; on one hand, light can be used to control the activity of the materials, and on the other hand, the nature of the materials limits the use of the light, the system requires additional accessories to generate light, and the material is not effective for applications in dark environments. There are also metal/metal oxide/2D nanostructures which can produce ions toxic to bacteria, or can introduce oxidative stress to the bacterial cells and be directly used as antimicrobial materials. These include metallic nanoparticles such as Ag, Cu, Au, etc. [17], nanocrystals of metal oxides such as CuO, Cu₂O, Fe₃O₄, etc., [16,17] hybrid metal nanoparticle/2D materials [29,30], and hybrid organic–inorganic nanostructures [31,32]. Several recent reviews on inorganic antimicrobial nanomaterials can be found in Ref. [16,17].

The antimicrobial nanomaterial should at the very least be characterized by three important properties: efficiency in killing bacteria, toxicity to normal cells, and ease/cost of production. That is, an ideal antimicrobial nanomaterial should inhibit the maximum amount of bacteria in a short period of time, this efficacy should be universal to most pathogenic bacteria, the materials should be less or not toxic to normal cells, and the fabrication or synthesis of the materials should be cheap and easy. Table 1 summarizes the performance of some popular direct antimicrobial nanomaterials (inorganic) reported in the literature against two of the most widely studied bacteria, *E. coli* and *S. aureus*. Both the Ag and Cu₂O nanoparticles (NPs) are found to be the most effective for killing *E. coli* and *S. aureus* as compared to other metal oxides. [33,34] It was reported that as little as 0.2 ppm of Ag NPs could inhibit 10⁵ CFU/mL of *E. coli* in 30 min, [33] while 50 µg/mL Cu₂O octahedral nanocrystals could eradicate 2 × 10⁷ CFU/mL *E. coli* in 5 min in a 0.9% saline water dispersion [34]. CuO is also a very effective antimicrobial material, as shown in Table 1 [35]. Other oxides take one or two days to achieve a reasonable bactericidal effect. However, the materials with high antimicrobial performance, i.e., the NPs of Ag, Cu₂O or CuO, were very toxic to human cells or in animal tests. Beer et al. showed that at 1.5 µg/mL total silver, the human pulmonary epithelial cells (A549) in vitro exposed to an Ag NP suspension containing a 69% silver ion fraction had a cell viability of 54% [36,37]. A recent study showed that the treatment with truncated octahedral Cu₂O particles caused a significant reduction in animal size and lifespan in the nematode worm animal model *Caenorhabditis elegans* [38]. Siddiqui et al. demonstrated that when the A549 cells were exposed to CuO NPs with concentrations of 10, 25, and 50 µg/mL, the cell viabilities were 75%, 66%, and 48%, respectively [39]. In short-term oral exposure in rats, the CuO NPs induced changes in hematology parameters and liver damage, and histopathological alterations were observed in the bone marrow, stomach and liver, mainly consisting of an inflammatory response, ulceration, and degeneration [40]. Clearly, highly efficient single component antimicrobial materials

are often accompanied by high toxicity due to the intrinsic antimicrobial mechanisms, which are not ideal for many applications.

Table 1. Summary of common inorganic antimicrobial materials and their best antimicrobial activity reported in the literature.

Material	Bacterial Strain	Reduction	Test Time	Reference
Silver (Ag)	<i>E. coli/S. aureus</i>	5 log	0.5 h/1.5 h	[33]
Copper oxide (CuO)	<i>E. coli</i>	3 log	3 h	[35]
Cuprous oxide (Cu ₂ O)	<i>E. coli</i>	7 log	5 min	[34]
Nitric oxide (NO)	<i>E. coli/A. baumannii/S. aureus</i>	8 log	24 h	[41]
Zinc oxide (ZnO)	<i>E. coli</i>	6 log	48 h	[42]
Copper (Cu)	<i>E. coli/S. aureus</i>	4 log	24 h	[43]

In order to circumvent the above issue, different strategies, such as surface modification, composite materials or hybrid materials, have been used to reduce the toxicity of these antimicrobial materials [16,44]. For example, Tran et al. incorporated CuO NPs into cellulose and chitosan to form biocompatible antimicrobial composites [45]. They demonstrated that the composites were effective in reducing the growth of drug-resistant bacteria (e.g., approximately 3 log growth reduction in *E. coli* and 5 log growth reduction in *Streptococcus agalactiae*) with 298 nmol/mg CuO loading after 16 h incubation [45]. Many results showed that these strategies could not only reduce the toxicity significantly, but also induce an appreciable reduction in antimicrobial efficiency. Additionally, many of the proposed strategies involve multiple material preparation steps, which are sometimes not easy to synthesize or are not cost effective. In addition, in most antimicrobial studies, only two to four different bacteria were studied simultaneously, which makes the data comparison very difficult (for instance, to compare bactericidal efficiency from different sources). Thus, it is still important to discover new materials that can effectively inhibit a broad range (strains) of bacteria but with less toxicity and easy synthesis.

Here, we demonstrate that a mixture of cuprous oxide (Cu₂O), iron oxide (Fe₂O₃) and copper iron oxide (CuFeO₂) NPs (designated as Cu_xFe_yO_z NPs), synthesized through a one-step microwave-assisted hydrothermal method, had a very high antimicrobial activity (>5 log reduction within 4 h) against a broad range of Gram-positive and Gram-negative bacteria, including drug-resistant bacteria. The materials can also inhibit the growth of these bacteria suspended in culture media, and the inhibition depends strongly on the bacteria strains. The cytotoxicity tests against mouse fibroblast cells suggest that these NPs were less toxic to the mammalian cells at a concentration lower than 1 mg/mL. Collectively, the results suggest that the Cu_xFe_yO_z NPs are an excellent antimicrobial material, with a high bactericidal effect, low toxicity and easy synthesis.

2. Materials and Methods

NP Synthesis and Characterizations: The Cu_xFe_yO_z NPs were produced through a microwave-assisted hydrothermal synthesis (Monowave 400, Anton Paar, Graz, Austria). In a typical synthesis, 0.242 g Cu(NO₃)₂·3H₂O (ACROS Organics, Fair Lawn, NJ, USA) and 0.404 g Fe(NO₃)₃·9H₂O (Alfa Aesar, Haverhill, MA, USA) were thoroughly dissolved into 10 mL deionized (DI) water. First, 10 mL 1 M NaOH solution was added into the mixture dropwise with constant stirring. Next, 500 µL 37% formaldehyde (J.T. Baker, Allentown, PA, USA) was added into the mixture. A measure of 4 mL of the resulting solution was transferred into a 10 mL SiC reaction tube and kept in the microwave chamber at 200 °C for 2 h. After cooling down, the synthesized sample was centrifuged, washed with DI water for 5 iterations, and oven dried at 60 °C overnight. Morphologies of the samples were investigated by a field-emission scanning electron microscope (FESEM, FEI Inspect F, ThermoFisher Scientific, Hillsboro, OR, USA) equipped with an energy dispersive X-ray spectroscopy. High resolution scanning electron microscopy (SEM) analysis was carried out using a Hitachi SU9000 STEM/SEM (Hitachi, Chatsworth,

CA, USA) at 30 kV, equipped with an Oxford solid state EDS detector (Oxford Instruments, Concord, MA, USA) to further investigate the morphologies and elemental composition of the $\text{Cu}_x\text{Fe}_y\text{O}_z$ NPs. The crystal structures of the prepared samples were characterized by an X-ray diffractometer (XRD; PANalytical X'Pert PROMRD, Malvern Panalytical, Malvern, UK) with a $\text{Cu K}\alpha$ source ($\lambda = 1.5405980 \text{ \AA}$) at 45 kV and 40 mA. The diffraction angle scanning range was 20° to 80° at an angular step of 0.02° . The Zeta potentials of the $\text{Cu}_x\text{Fe}_y\text{O}_z$ NPs were measured by a Malvern Zetasizer Nano ZS system (Malvern Panalytical, Westborough, MA, USA) at 25°C . The dye degradation experiments were performed using methyl orange (MO) and methylene blue (MB) aqueous solutions with a concentration of $30 \mu\text{M}$ at room temperature. All experiments were performed with a concentration of the $\text{Cu}_x\text{Fe}_y\text{O}_z$ NPs at 0.5 mg/mL , and a fixed volume $V = 20 \text{ mL}$ of dye solutions. The reaction systems were kept in the dark with constant stirring. At each time interval (2, 4, 6, 8, 10 and 24 h), an aliquot sample was withdrawn and centrifuged at $12,000 \times g$ rpm to remove the NPs, and the concentration change of MO and MB in the remaining solution was investigated by UV-Vis.

Antimicrobial activity tests: The antimicrobial performance of the samples was tested on various bacterial strains (see Table S1 of SI). The bacterial stocks were activated in fresh liquid media (trypticase soy broth (TSB) for *E. coli* B and *S. aureus*; Luria Bertani broth (LB) for *E. coli* O157:H7, *Klebsiella pneumoniae* 4/484, *K. pneumoniae* ATCC-BAA-2472, *Listeria monocytogenes*, *Salmonella enterica* serovar Typhimurium ATCC-700408, and *Shigella flexneri*) overnight at 37°C with shaking (250 rpm). *H. pylori* cells were routinely grown on blood agar (BA) plates under microaerobic conditions (5% O_2 , 5% CO_2 , 90% N_2). For the antimicrobial tests with bacterial cells in phosphate buffered saline (PBS), bacterial cells grown in the media described above were harvested by centrifugation at $4000 \times g$ rpm for 5 min, washed twice with PBS, and finally re-suspended in PBS. For *E. coli* B and *S. aureus* tests, 1 mg of $\text{Cu}_x\text{Fe}_y\text{O}_z$ NPs was directly suspended in the bacteria suspension. For other bacterial strains, the cells were first standardized to an OD_{600} of 2 in PBS ($\sim 10^9$ to 2×10^9 CFU/mL depending upon strains), then 0.25 mL of each cell suspension was diluted with either 0.25 mL of PBS as controls or 0.25 mL of 2 mg/mL $\text{Cu}_x\text{Fe}_y\text{O}_z$ NPs. The mixtures of bacteria and $\text{Cu}_x\text{Fe}_y\text{O}_z$ NPs were incubated at 37°C with shaking (200 rpm). Aliquots were withdrawn at various time intervals (15, 30, 60, 120, and 240 min, respectively), and 10-fold serially diluted in PBS. The dilutions were plated on media plates and incubated at 37°C for 12 to 16 h. *H. pylori* cell dilutions were incubated on BA plates for 3 to 5 days under microaerobic conditions. All antimicrobial activity tests were done in triplicate.

Bacterial growth inhibition tests: For growth inhibition tests, bacterial cells were inoculated into fresh media with $\text{Cu}_x\text{Fe}_y\text{O}_z$ NP suspensions. For *E. coli* B and *S. aureus* tests, 10 mg $\text{Cu}_x\text{Fe}_y\text{O}_z$ NPs were briefly suspended in 0.1 mL PBS first, then added into 9.9 mL TSB (final NPs concentration was 1 mg/mL). Next, a 10 μL bacteria suspension was inoculated into the media–NPs mixture and kept at 37°C for 12 to 16 h with shaking (250 rpm). For the *K. pneumoniae* BAA-2472, *S. Typhimurium* 700408, and *S. flexneri* experiments, a 2 μL bacteria suspension (corresponding to approximately 2×10^6 cells) was inoculated in 500 μL TSB with 1 mg/mL $\text{Cu}_x\text{Fe}_y\text{O}_z$ NPs. For *H. pylori*, cells were grown on BA plates, harvested, and resuspended in 100 μL of brain–heart infusion with 0.4% β -cyclodextrin (BHI- β c) to a final concentration of approximately 10^7 cells, and were then inoculated into 2 mL BHI- β c supplemented with 0.1 mL 20 mg/mL $\text{Cu}_x\text{Fe}_y\text{O}_z$ NPs in PBS (final NPs concentration was 1 mg/mL). These bacteria–media–NP mixtures were then incubated at 37°C for 18 h under aerobic (all strains except *H. pylori*) or microaerobic (for *H. pylori*) conditions with constant rocking or shaking. After co-incubating with NPs in media, an aliquot amount of the mixture was withdrawn from each sample and 10-fold diluted in PBS. The dilutions were plated onto agar plates and incubated at 37°C as described above. Control groups were performed with an equal volume of PBS to replace the $\text{Cu}_x\text{Fe}_y\text{O}_z$ NP suspension. All bacterial growth inhibition tests were done in triplicate.

Cytotoxic activity tests: The cytocompatibility test of the $\text{Cu}_x\text{Fe}_y\text{O}_z$ NPs was performed using a standard WST-8 dye-based assay in accordance with the manufacturer's recommendations (Sigma-Aldrich). During the experiment, mouse fibroblast cells were grown in a 75 cm^2 T-flask and incubated in a humidified CO_2 incubator for 6–7 days at 37°C until 80–90% confluent. Thereafter,

cells were detached using 0.5% trypsin EDTA, counted via trypan blue assay (0.4%) (EVE Automatic cell Counter) and 100 μ L of 5000 cells/mL were seeded in a 96 well plate. The plate was kept for 24 h at 37 °C in a CO₂ incubator to allow cells to fully grow and attach to the surface. In parallel, a 1 mg/mL or a 10 mg/mL Cu_xFe_yO_z solution was prepared in Dulbecco's Modified Eagle's Medium (DMEM). The cells were allowed to grow in the well plate at 37 °C for 24 h. After 24 h, the medium was replaced with the prepared medium containing 1 mg/mL or 10 mg/mL Cu_xFe_yO_z. The cells grown in the well plate in the absence of Cu_xFe_yO_z NPs were used as a control group ($n = 8$ for each condition). After 24 h of the exposure, 10 μ L of WST-8 dye was added to each of the wells containing cells. Viable cells converted the WST-8 dye into a yellow-colored formazan product. The DMEM medium was used as a blank to baseline the background. The absorbance of formazan was measured at 450 nm with a BioTek spectrophotometer as a measure of cell viability. The relative change in cell viability was calculated considering a 100% control viability. All cytotoxic activity tests were done in triplicate.

Statistical analysis: all results shown are means and standard deviations for experiments done in triplicate. When required, statistical analysis was done using Student's *t*-test.

3. Results

3.1. Synthesis and Characterizations of Cu_xFe_yO_z NPs

During the microwave hydrothermal synthesis, we kept the amounts of the Cu(NO₃)₂·3H₂O, Fe(NO₃)₃·9H₂O and NaOH the same, and systematically changed the volume of 37% formaldehyde from 200 μ L to 500 μ L to obtain different Cu_xFe_yO_z NPs. We denote the name of the samples as S200, S250, . . . , S500, which correspond to the volumes of formaldehyde 200 μ L, 250 μ L, . . . , and 500 μ L, respectively. Figure 1 shows the representative SEM images of the resulting Cu_xFe_yO_z NPs. Despite the detailed synthesis conditions, the Cu_xFe_yO_z NPs consist of NPs of different sizes and shapes, including rod-shaped, plate-like-shaped, and other irregular shapes, and the average size of the NPs became smaller and smaller when more and more formaldehyde was added. In fact, based on the scanning electron microscopy (SEM) images and the dynamic light scattering (DLS) measurements, the average size of the NPs decreased monotonically as a function of the amount of formaldehyde added (see Figure S1 of Supporting Information (SI)) [46]. The crystallinity of the NPs was characterized by X-ray diffraction (XRD) as shown in Figure 2A. All 6 samples are a mixture of multiple oxides, as revealed by the XRD pattern—the 2 θ peaks at 24.1°, 29.6°, 33.1°, 40.8°, 49.4° and 54.0° correspond to the (012), (220), (104), (113), (024), and (116) crystal planes of α -Fe₂O₃ (indicated by "*" in Figure 2A), the XRD peaks at 38.7° and 48.7° are due to the (200) and (202) crystal planes of CuO (indicated by "o"), the peaks at 42.2° and 61.3° are the (200) and (220) crystal planes of Cu₂O (indicated by "&"), and the peaks at 31.2°, 35.6°, 40.2°, and 55.1° are from the (006), (012), (104), and (018) crystal planes of CuFeO₂. After careful analysis of the XRD peak positions, one finds that only the samples S200 and S500 are a mixture of three oxides, i.e., CuFeO₂, CuO, and Fe₂O₃ for S200, and CuFeO₂, Cu₂O, and Fe₂O₃ for S500. The other four samples are a mixture of all four different oxides, i.e., CuFeO₂, CuO, Cu₂O, and Fe₂O₃. The formation of the Cu_xFe_yO_z NPs could be the intermediate product towards the formation of single-phase CuFeO₂ NPs, since the reaction time for the synthesis was very short (2 h). For example, the rhombohedral CuFeO₂ crystals reported by Qiu et al. were formed under the prolonged hydrothermal reaction times of 24 h, 48 h, and 64 h, respectively [47], while Abdelhamid et al. spent 24 h to obtain CuFeO₂ NPs capped with glycerol [48]. The XRD patterns can also be used to roughly estimate the relative composition ratio of the four oxides according to a semiquantitative analysis utilizing the Rietveld program from the FullProf software, [49–52] and the results are shown in Figure 2B. For sample S200, the relative compositions of CuFeO₂, CuO, and Fe₂O₃ are 54%, 26%, and 20%, respectively, while for S500, the ratios for CuFeO₂, Cu₂O, and Fe₂O₃ are 36%, 28%, and 36%, respectively. Thus, the sample S500 has an almost equal amount of the three oxides. Among all six samples, the sample S350 has the highest composition of Cu₂O, sample S200 has the highest composition of CuFeO₂ and CuO, and sample S500 has the most Fe₂O₃ in its composition. The catalytic

performance of $\text{Cu}_x\text{Fe}_y\text{O}_z$ NPs was characterized by a dye degradation against methyl orange (MO) under the dark condition through a UV-Vis spectroscopy measurement, and the normalized optical absorbance peak α at the characteristic wavelength $\lambda = 464$ nm of MO solution against the decay time t is plotted in Figure 3. The sample S200 shows almost no decay of MO, while S500 demonstrates the highest degradation, i.e., almost 80% of MO was decomposed after 10 h. This indicates that the sample S500 exhibits the highest catalytic activity among all the $\text{Cu}_x\text{Fe}_y\text{O}_z$ NPs synthesized. Based on previous literature, the high catalytic performance of a material usually links to a high antimicrobial activity [53,54]. Therefore, in the following, we will concentrate on the sample S500.

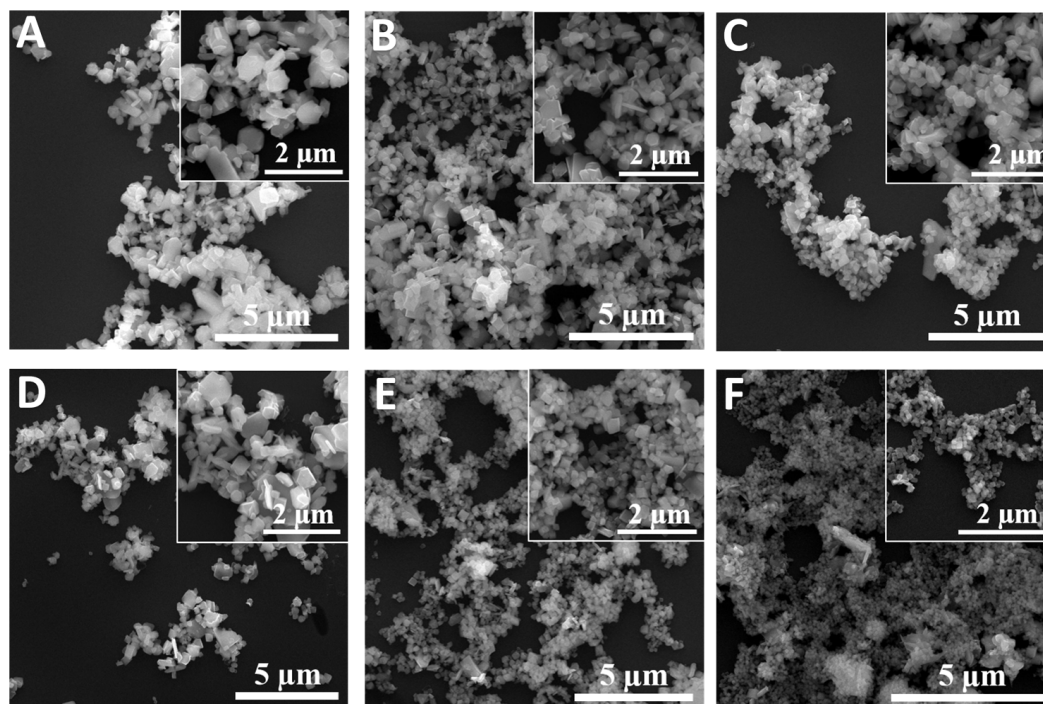


Figure 1. Representative SEM images of $\text{Cu}_x\text{Fe}_y\text{O}_z$ NPs designated by CH_2O addition in synthesis. (A) S200; (B) S250; (C) S300; (D) S350; (E) S400; and (F) S500.

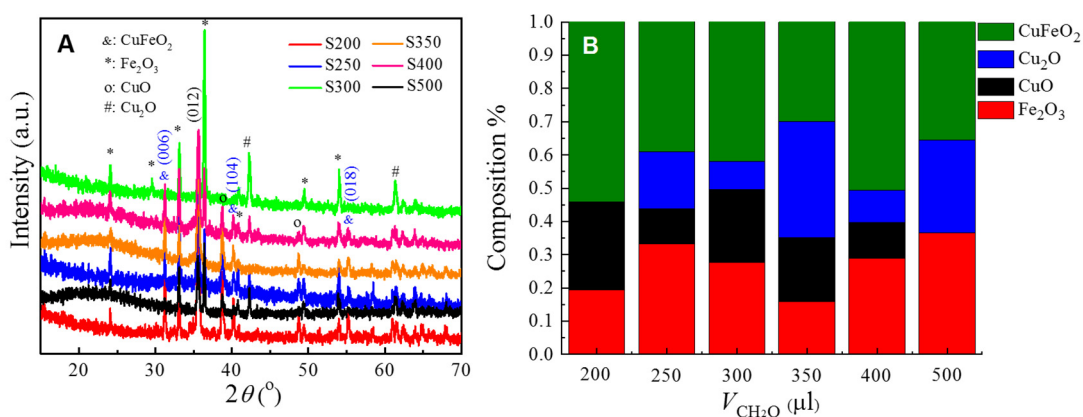


Figure 2. (A) The XRD patterns of the six samples S200 to S500. The diffraction peaks from CuFeO_2 , CuO , Cu_2O , and Fe_2O_3 are indicated in the plot. (B) The relative compositions of CuFeO_2 , CuO , Cu_2O , and Fe_2O_3 in each samples extracted from the Rietveld program.

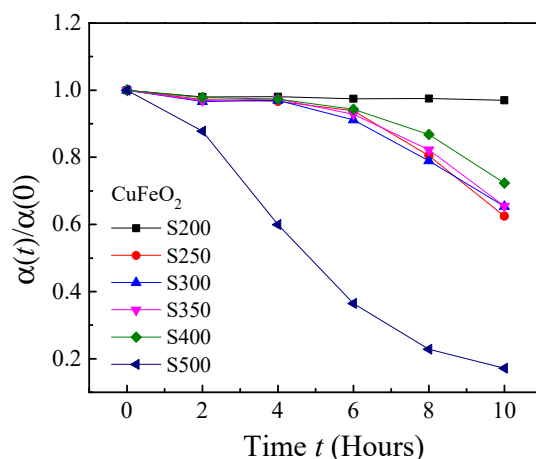


Figure 3. Catalytic activity of different $\text{Cu}_x\text{Fe}_y\text{O}_z$ NP samples: remaining concentrations of methyl orange after exposure to $\text{Cu}_x\text{Fe}_y\text{O}_z$ NP samples. Dark conditions were maintained throughout the entire process.

The as-synthesized sample S500 comprises various shapes of particles, such as cubic, flake, and irregular shapes (Figure 1F), with a mean size of 100 ± 20 nm in diameter. The higher magnification scanning electron micrograph (SEM) and the energy dispersive X-ray spectroscopic (EDS) mapping (Figure 4) show that oxygen is uniformly distributed on all structures, but the Fe and Cu atoms are not distributed evenly. There are greater Fe contents in the cubic NPs, while the strip structures are mainly composed of Cu contents. According to the XRD analysis in Figure 2, the strip structures in Figure 4 could mainly be the Cu_2O , while the other shaped NPs are Fe_2O_3 and CuFeO_2 . In addition, the sample S500 shows strong dye degradation activities against the cationic dye, MO ($\sim 90\%$ reduction in 24 h), but is less effective on the anionic dye, methylene blue (MB) ($\sim 8\%$ reduction in 24 h (see Figures S2 and S3 in SI)) when tested with 0.5 mg/mL NP suspensions in the dark after a 24 h treatment. This could be attributed to the fact that the decomposition of MB mainly occurs through reduction reactions [55], while the decomposition of MO is mainly due to oxidation reactions [56]. That is, the results suggest that the as-synthesized $\text{Cu}_x\text{Fe}_y\text{O}_z$ NPs are efficient oxidizing agents. Similar properties of other $\text{Cu}_x\text{Fe}_y\text{O}_z$ NP samples are summarized in Table S2.

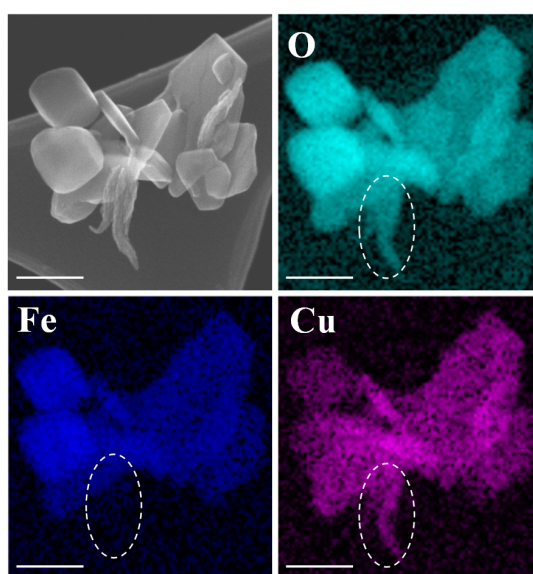


Figure 4. EDS mapping (elements of O, Fe, and Cu) of a $\text{Cu}_x\text{Fe}_y\text{O}_z$ (S500) NP cluster. The scale bars represent 100 nm. The dashed-oval outlines the Cu_2O NPs.

3.2. Antimicrobial Characterizations of S500

The outstanding MO oxidizing activity suggests that the S500 should have good antimicrobial properties. To test this hypothesis, antimicrobial tests were carried out using nine important pathogenic bacterial strains, including Gram-positive species such as *S. aureus* Rosenbach ATCC-6538 and *L. monocytogenes*, and Gram-negative species, such as enterohemorrhagic *E. coli* (EHEC) strain O157:H7, *K. pneumoniae* strain 4/484 and strain ATCC-BAA-1472, *S. Typhimurium* ATCC-700408, *H. pylori* X47, and *S. flexneri* strain 2457T; among those are the multidrug-resistant (MDR) *K. pneumoniae* 4/484 and BAA-2472, and *S. Typhimurium* 700408. The nonpathogenic *E. coli* strain B was used as a reference (the details on the bacteria strains can be found in Table S1 of SI). The final $\text{Cu}_x\text{Fe}_y\text{O}_z$ NP (S500) concentration was 1 mg/mL throughout all experiments. To ensure that the sample S500 shows better antimicrobial activity, antimicrobial tests against *E. coli* B for both S200 and S500 with different concentrations were conducted. The results are shown in Figure S4 of SI, which confirms that sample S500 has better antibacterial activity. Figure 5 shows the plots of the time-dependent bacterial survival loads, while Table 2 summarizes the significant bacterial killing efficiency observed for different bacterial strains. The $\text{Cu}_x\text{Fe}_y\text{O}_z$ NPs (S500) show high antimicrobial activity against almost all the bacterial strains tested. First, the $\text{Cu}_x\text{Fe}_y\text{O}_z$ NPs can kill both Gram-negative and Gram-positive bacteria very effectively. The results showed a more than 9 log reduction in 0.25 h (15 min) for *E. coli* B and a 10 log reduction within 1 h for *S. aureus*. For other bacteria, such as *E. coli* O157:H7 and *L. monocytogenes*, a more than 7 log reduction was observed upon 4 h of $\text{Cu}_x\text{Fe}_y\text{O}_z$ NPs exposure. The results indicated that these nanoparticles could effectively kill the bacterial cells within a very short exposure term. Compared to the best antimicrobial activities of other inorganic nanostructures shown in Table 1, only Ag NPs or Cu_2O NPs can achieve similar or better results. However, both Ag and Cu_2O NPs are highly toxic to host cell lines, while the $\text{Cu}_x\text{Fe}_y\text{O}_z$ NPs are not (see toxicity test later). In addition, the $\text{Cu}_x\text{Fe}_y\text{O}_z$ NPs also exhibited rapid and effective antimicrobial activities against highly infectious drug-resistant strains—the biocidal efficiencies of the $\text{Cu}_x\text{Fe}_y\text{O}_z$ NPs against MDR *K. pneumoniae* 4/484, BAA-2472, and *S. typhimurium* 700408 showed an 8.4 and 6.9 log reduction, respectively, in 4 h, and a 7.2 log reduction in 2 h, respectively.

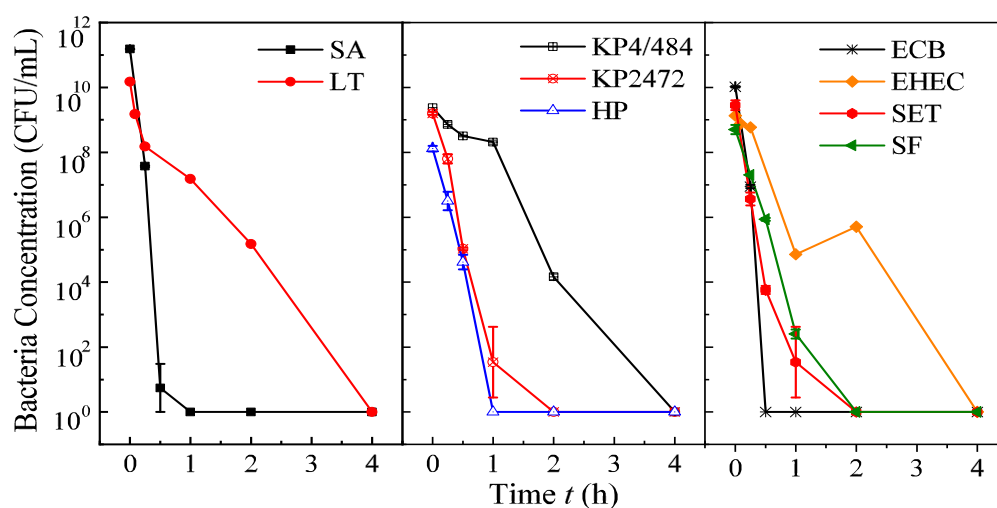


Figure 5. Antimicrobial tests of $\text{Cu}_x\text{Fe}_y\text{O}_z$ NPs (1 mg/mL in PBS) against various pathogenic bacteria. The acronyms for bacteria are listed in Table 2. Results represent 3 independent challenge experiments (2 for KP4/484) and are expressed as mean and standard deviation of bacterial concentration (in CFU/mL).

Table 2. Antimicrobial activity of the $\text{Cu}_x\text{Fe}_y\text{O}_z$ NPs (bacterial cells were suspended in 1X PBS).

Bacteria Strain	Log Reduction	Time/h
<i>E. coli</i> B (ECB) (−)	>9.0	0.25
<i>S. aureus</i> (SA) (+)	>10.2	1
<i>K. pneumoniae</i> 4/484 (KP4/484) (−)	>8.4	4
<i>E. coli</i> O157:H7 (EHEC) (−)	>7.1	4
<i>Listeria</i> (LT) (+)	>9.2	4
<i>K. pneumoniae</i> BAA-2472 (KP2472) (−)	>6.9	2
<i>S. Typhimurium</i> 700408 (SET) (−)	>7.2	2
<i>H. pylori</i> X47 (HP) (−)	>5.8	1
<i>S. flexneri</i> 2457T (SF) (−)	>6.4	2

+: Gram-positive bacteria; −: Gram-negative bacteria.

The high antimicrobial activity of the S500 was also demonstrated upon bacterial incubation under favorable culture conditions (bacteriostatic effect) when cells were incubated with the inhibitor from the start of culture. Both the $\text{Cu}_x\text{Fe}_y\text{O}_z$ NPs and bacteria were incubated in adequate fresh broth culture media, and bacterial growth was monitored by CFU counting after serial dilutions. The results are summarized in Figure 6. These NPs inhibited the growth of the bacteria under favorable growth conditions. As such, *H. pylori* growth was completely inhibited after 24 h co-culturing in the BHI- β c media; in contrast, *H. pylori* achieved a concentration as high as 10^8 CFU/mL in the control group. For the test against MDR *K. pneumoniae* BAA-2472, a 4 log reduction was obtained after 24 h growth. Similar results were obtained for *S. flexneri*, *S. aureus* and *E. coli*—these bacteria were all subject to inhibition by $\text{Cu}_x\text{Fe}_y\text{O}_z$ NPs. It is expected that, since this is a competition between the cell growth and cell killing, the number of bacterial cells that survived the bacteriostatic effect may be much greater than those in the antimicrobial tests. The tests further suggest that the S500s are promising antimicrobial agents.

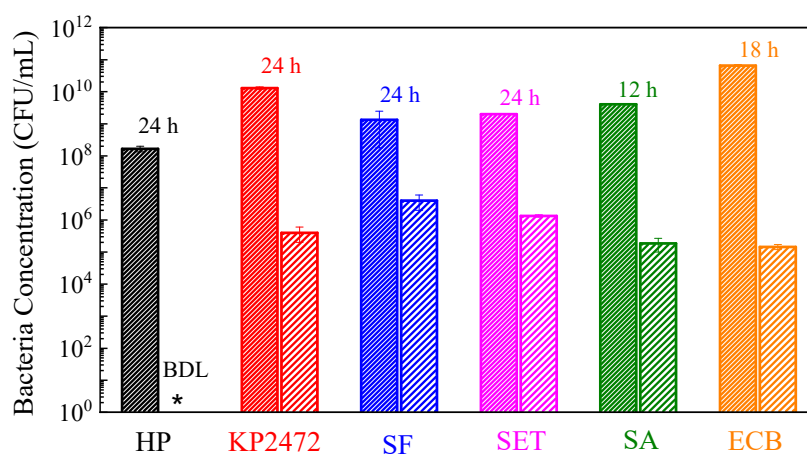


Figure 6. Bacterial inhibition tests: co-culturing bacteria with 1 mg/mL $\text{Cu}_x\text{Fe}_y\text{O}_z$ NPs in corresponding growth media. The results represent 3 independent growth experiments and are expressed as mean and standard deviation of CFU/mL (at the time indicated above each column). BDL: below detection limit (<200 CFU/mL). For each bacterial species, the bacterial concentration after $\text{Cu}_x\text{Fe}_y\text{O}_z$ treatment is significantly lower compared to the bacterial concentration obtained without treatment ($p < 0.01$, Student's t test).

The antimicrobial mechanism of the $\text{Cu}_x\text{Fe}_y\text{O}_z$ NPs (S500) is not yet well understood. According to the composition analysis shown in Figure 2, there are three kinds of NPs in the mixture: Cu_2O , CuFeO_2 , and Fe_2O_3 . Cu_2O NPs are well-known antimicrobial nanomaterials [34] and recent reports show that CuFeO_2 NPs can kill viruses [47] and fungi [48]. The Fe_2O_3 NPs are a photocatalytic material and they can only show antimicrobial activity when illuminated by light with energy higher than the

energy band gap [28]. Thus, we hypothesize that the antimicrobial properties might mostly originate from the Cu_2O and CuFeO_2 . For these two materials, the antimicrobial properties are attributed to a Cu^+ species in the compounds [47,48]. To gain a better insight, we have also synthesized two control NPs (the Fe_2O_3 and Cu_2O NPs) under similar conditions, and their characterizations are presented in Section S5 of SI. Their antimicrobial activities against KP2472, SET and SF are shown in Figure 7. The Fe_2O_3 NPs alone do not demonstrate any antimicrobial effect, while the biocidal efficiency values of the Cu_2O NPs for KP2472, SET and SF are 9 log, 9 log and 8 log reductions in 30 min, 15 min, and 60 min, respectively. This shows that the Cu_2O NPs are effective antimicrobial agents, which is consistent with results reported in the literature. [34,57,58] Compared to the antimicrobial activity against corresponding bacteria for S500, the Cu_2O NPs are more effective. Since the S500 is a mixture of Cu_2O , CuFeO_2 and Fe_2O_3 NPs, such a result is expected, which means that the Cu_2O NPs in S500 could play a major role in its antimicrobial activity.

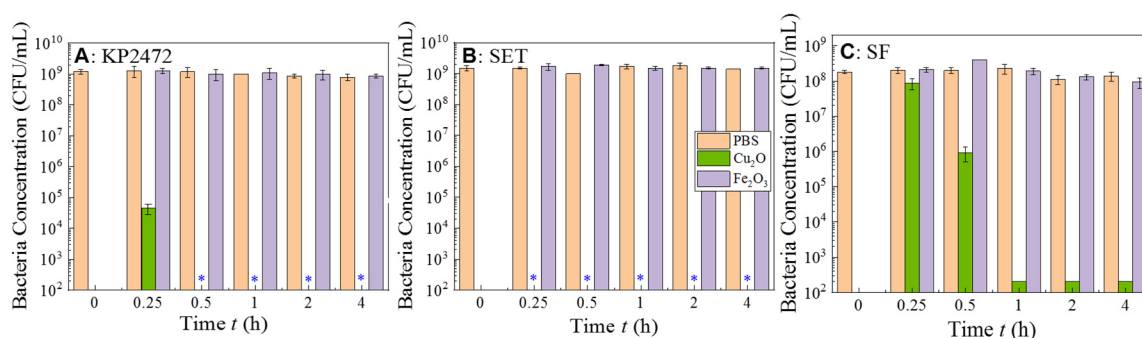


Figure 7. Antimicrobial tests of 1 mg/mL control Fe_2O_3 and Cu_2O NPs against various pathogenic bacteria (A) *K. pneumoniae* (KP2472), (B) *S. Typhimurium* (SET), and (C) *S. flexneri* (SF). These tests were carried out in the dark. The results represent 3 independent growth experiments and are expressed as mean and standard deviation of CFU/mL. The treatment leading to a significant reduction in bacterial concentration is indicated by a blue asterisk ($p < 0.01$ Student's t test).

The role of CuFeO_2 NPs is difficult to determine since we could not directly synthesize pure CuFeO_2 NPs via the microwave-assisted hydrothermal method. Based on previous reports [47,48], the CuFeO_2 NPs should also have a strong antimicrobial effect. In fact, according to a comparison study by Antonoglou et al., the CuFeO_2 NPs exhibited less antimicrobial activity than the Cu_2O NPs, but their cytotoxicity was also lower [59]. Since the S500 sample has 36% CuFeO_2 , 0% CuO , 28% Cu_2O and 36% Fe_2O_3 (Figure 2b), one could use a control mixture of Fe_2O_3 and Cu_2O NPs (their crystalline properties are shown in Figure S5) to indirectly explore the effect of CuFeO_2 NPs. The control mixture had a mass ratio of Cu_2O NPs: Fe_2O_3 NPs = 28:36, with a total NP concentration of 0.64 mg/mL (i.e., mimicking the S500 without CuFeO_2) against KP2472 and SET, and the results are shown in Figure 8. The antimicrobial activity values of the control mixture for KP2472 and SET are 9 log and 6 log reductions in 2 h and 1 h, respectively. Clearly, the control mixture also has a higher antimicrobial activity as compared to that of sample S500, which indicates that the sample S500 is not a simple mixture of Cu_2O , CuFeO_2 , and Fe_2O_3 NPs. In fact, based on the SEM image shown in Figure 4, the mixture of Cu_2O , CuFeO_2 and Fe_2O_3 NPs in sample S500 forms super clusters, and the three different NPs physically join together to form complicated hetero-interfaces. These hetero-interfaces could form semiconductor junctions due to the energy band realignment, and change the electron structures of the materials so that the corresponding catalytic activity will be greatly changed compared to that of pure Cu_2O or Fe_2O_3 NPs. The control mixture of Cu_2O and Fe_2O_3 NPs is a simple blend, and they act separately on bacteria.

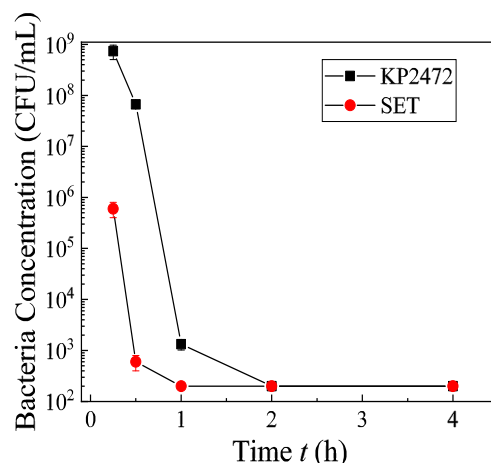


Figure 8. Antimicrobial tests of a mixture of the control Fe₂O₃ and Cu₂O NPs against KP2472 and SET in a dark environment. The results represent 3 independent growth experiments and are expressed as mean and standard deviation of CFU/mL.

The bacteria growth inhibition tests of the control Cu₂O and Fe₂O₃ NPs (1 mg/mL) were performed against HP, and the results are shown in Figure 9. Similar conclusions can be drawn for the antimicrobial tests: the Fe₂O₃ NPs do not inhibit the bacteria growth, while the Cu₂O NPs inhibit the growth significantly (i.e., 9 log inhibition for 1 h).

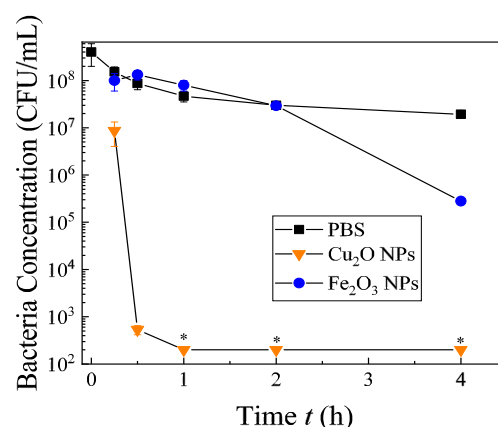


Figure 9. Bacteria inhibition tests for 1 mg/mL control Fe₂O₃ and Cu₂O NPs in corresponding growth media. “*”: ND/below detection limit (200 CFU/mL). These tests were carried out in a dark environment. The results represent 3 independent inhibition experiments and are expressed as mean and standard deviation of CFU/mL.

It is well-known that copper ions are capable of killing microorganisms effectively by denaturation (enzyme, protein, etc.) or oxidation mechanisms [60,61]. It was reported that Cu₂O nanocrystals could generate reactive oxygen species (ROS) through biochemical processes [62]. In general, during these biochemical processes, as a redox-active transition metal, Cu can cycle between two redox states—oxidized cupric and reduced cuprous states. It is suggested that Cu can react with endogenous H₂O₂ to generate hydroxyl radicals in a process analogous to the Fenton reaction, and it can also catalyze the transfer of electrons from a donor biomolecule to an acceptor such as O₂ to generate O₂^{-•} or hydroxyl radicals (•OH) [46,62]. These ROS are toxic to bacterial cells, which can disrupt specific microbial processes. The direct effects of ROS on bacterial cells are mediated by the increasing production of ROS, which can lead to the oxidative damage of the cellular compounds [63]. Studies show that the ROS could damage cell membranes, subsequently causing cytoplasmic metabolites to leak and ion gradients to collapse, leading to cell death [35,64]. Furthermore, the ROS can destroy key

macromolecules, such as the iron–sulfur cluster components of enzymes, to disintegrate and oxidize amino acid residues within proteins, generate lipid peroxides, and damage DNA [64,65]. On the other hand, Antonoglou et al. showed that the CuFeO_2 NPs had a better biocompatibility for DNA and were less effective in protein denaturing [59]. The addition or clustering of CuFeO_2 and Fe_2O_3 NPs with Cu_2O NPs in S500 significantly slows down the bacteria inhibition process.

3.3. Cytotoxicity of the $\text{Cu}_x\text{Fe}_y\text{O}_z$ NP Sample S500

It is also well-known that a high concentration of ROS and Cu ions can also trigger damage on mammalian cells. Thus, the cytotoxicity of the $\text{Cu}_x\text{Fe}_y\text{O}_z$ NPs (S500) against mammalian cells needs to be explored. The cytotoxicity test of the $\text{Cu}_x\text{Fe}_y\text{O}_z$ NPs was performed by the exposure of mouse fibroblast cells to different concentrations of $\text{Cu}_x\text{Fe}_y\text{O}_z$ NPs at 37 °C for 24 h. As shown in Figure 10A, fibroblasts treated with 10 mg/mL $\text{Cu}_x\text{Fe}_y\text{O}_z$ NPs could only retain less than 10% cell viability. However, when treated with 1 mg/mL $\text{Cu}_x\text{Fe}_y\text{O}_z$ NPs (which was the concentration used for antimicrobial activity tests, see Figures 5 and 6 and Table 2), about 74% of the fibroblasts remained viable. Results for control NPs (1 mg/mL for Cu_2O and Fe_2O_3 NPs, and 0.64 mg/mL for the Cu_2O and Fe_2O_3 NP mixture) are shown in Figure 10B. For Cu_2O NPs, the number of viable cells rapidly decreased to $20 \pm 7\%$; compared to Cu_2O NPs, the cell viability was moderately affected by the presence of Fe_2O_3 NPs. The mixed Cu_2O and Fe_2O_3 NPs, however, exhibited a high degree of cytotoxicity (the viability goes down to $30 \pm 7\%$). Thus, it becomes increasingly evident that the cytotoxic effects elicited on the fibroblast cells are primarily due to Cu_2O NPs. Clearly, the cytotoxicity result for $\text{Cu}_x\text{Fe}_y\text{O}_z$ NPs (S500) is comparable to that of the control Fe_2O_3 NPs. In comparison to other high-efficiency antimicrobial inorganic materials, for example the CuO NPs, it was reported that at a concentration of 80 $\mu\text{g/mL}$, the CuO NPs were toxic to lung cells and could also cause DNA damage to the cells [66]. Thus, many efforts have been made to cap the CuO or Cu_2O NPs with polymers or ligands to reduce the toxicity. However, such a coating could also decrease the antimicrobial activity. Our results suggest that the $\text{Cu}_x\text{Fe}_y\text{O}_z$ NPs (S500) are toxic to the mouse fibroblasts only when used at a very high concentration (10 mg/mL). The cytotoxicity of the $\text{Cu}_x\text{Fe}_y\text{O}_z$ NPs at high concentrations also indirectly implies that the Cu^+ from the mixture could play an important role in antimicrobial activity. However, at a lower concentration of 1 mg/mL, they are much less toxic. At this concentration (1 mg/mL), $\text{Cu}_x\text{Fe}_y\text{O}_z$ NPs are found to have highly efficient antimicrobial activities against a wide range of microorganisms. As such, the low toxicity to mammalian cells combined with the strong antimicrobial activity against some of the most important human pathogens suggest that the $\text{Cu}_x\text{Fe}_y\text{O}_z$ NPs inhibitory agents could be broadly applicable, such as for water treatment applications, wound treatments, or when used as coatings for medical devices.

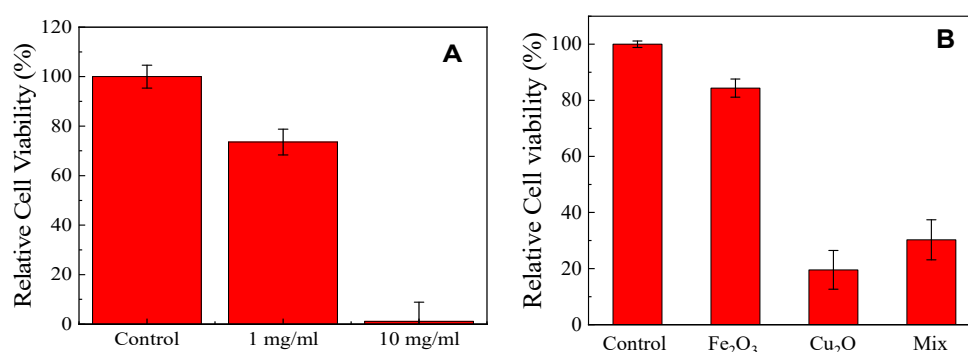


Figure 10. (A) Cytotoxicity of the $\text{Cu}_x\text{Fe}_y\text{O}_z$ NPs against mouse fibroblast cells: cell viability after cells exposed to $\text{Cu}_x\text{Fe}_y\text{O}_z$ NPs at 0 mg/mL (control), 1 mg/mL, and 10 mg/mL for 24 h. (B) Cytotoxicity of the control NPs against mouse fibroblast cells: cell viability after cells exposed to NPs at 1 mg/mL for 24 h. The results represent 3 independent experiments and are expressed as mean and standard deviations of relative cell viability (compared to control).

4. Conclusions

In summary, we have synthesized mixed composition $\text{Cu}_x\text{Fe}_y\text{O}_z$ NPs using a facile one-step microwave assisted hydrothermal synthesis. The resulting samples were a mixture of CuFeO_2 , CuO , Cu_2O and Fe_2O_3 , and all of them show catalytic activity against MO solutions. The sample S500 showed the best MO-degradation among all of the samples, and was selected to conduct the detailed antimicrobial study. The EDS and XRD results confirmed that the S500 sample had a composition of Cu_2O , Fe_2O_3 and CuFeO_2 . The $\text{Cu}_x\text{Fe}_y\text{O}_z$ NPs also showed highly effective antimicrobial activity (>5-fold log reduction within 4 h) against different Gram-positive and Gram-negative bacteria, including three drug-resistant strains. These antimicrobial activities are among the highest reported in the literature. Two of the inhibited bacteria strains are within the highly recalcitrant ESKAPE group of pathogenic bacteria, the bacterial group causing the majority of nosocomial infections throughout the world [67]. Moreover, *S. aureus*, *K. pneumoniae* and *E. coli* strains cause nearly 30% of all nosocomial infections in the USA [68]. When co-culturing the NPs with bacteria in growth media, the NPs can also eliminate bacteria growth. The toxicity test showed that the mouse fibroblast cell viability was about 74% when exposed to 1 mg/mL $\text{Cu}_x\text{Fe}_y\text{O}_z$ NPs for 24 h, as compared to the 69% viability of 1.5 $\mu\text{g/mL}$ Ag NPs [36,37] and the 75, 66 and 48% viability of 10, 25, and 50 $\mu\text{g/mL}$ CuO NPs [39]. Thus, $\text{Cu}_x\text{Fe}_y\text{O}_z$ NPs have low toxicity and could selectively target bacteria, which is a great advantage compared to other inorganic antimicrobial materials. Furthermore, when compared to silver NPs, the $\text{Cu}_x\text{Fe}_y\text{O}_z$ NPs are inexpensive and chemically stable. Evidently, the $\text{Cu}_x\text{Fe}_y\text{O}_z$ NPs are an excellent antimicrobial material. However, there are still many unanswered questions for this study, as follows: (1) Why do the $\text{Cu}_x\text{Fe}_y\text{O}_z$ NPs have a high antimicrobial efficacy but low toxicity, while a mixture of Cu_2O and Fe_2O_3 NPs is still highly toxic? To answer this question, one needs to have a good understanding of the detailed microstructure of the $\text{Cu}_x\text{Fe}_y\text{O}_z$ NPs, as well as of how the particle interacts with the bacteria cells. (2) What is (are) the mechanism(s) for the bactericidal effect? Is it really caused by Cu^+ species or by the production of reactive oxygen species? Or other mechanisms? (3) Is the S500 sample the best antimicrobial material out of similar fabrication strategies? We have only done a very limited investigation on $\text{Cu}_x\text{Fe}_y\text{O}_z$ NP synthesis by varying the amount of formaldehyde in the reagents. It is unknown what would happen if the concentrations of the $\text{Cu}(\text{NO}_3)_2 \cdot 3\text{H}_2\text{O}$, $\text{Fe}(\text{NO}_3)_3 \cdot 9\text{H}_2\text{O}$ and NaOH were changed. Thus, a more systematic study on synthesis conditions may find a better antimicrobial material. Nevertheless, our current studies do show that the synthesis method of $\text{Cu}_x\text{Fe}_y\text{O}_z$ NPs is simple. The raw materials for synthesis are abundant, and these $\text{Cu}_x\text{Fe}_y\text{O}_z$ NPs are an excellent candidate for antimicrobial applications, such as antimicrobial cream, spray, and coating, as well as assays for disinfections or water treatment.

Supplementary Materials: The following are available online at <http://www.mdpi.com/2079-4991/10/11/2294/s1>: Table S1: Bacterial strains used in this study. Table S2: Summary of the properties of $\text{Cu}_x\text{Fe}_y\text{O}_z$ NP samples. Figure S1: Size comparison between SEM data and dynamic light scattering (DLS). Figure S2: The normalized and time-dependent optical absorption $\alpha(t)/\alpha(0)$ of the characteristic peaks of MO and MB after mixed with S500. Figure S3: The time-dependent UV-Vis spectra of (a) methyl orange and (b) methylene blue after being mixed with S500 $\text{Cu}_x\text{Fe}_y\text{O}_z$ NPs in the dark for 24 h. Figure S4: Concentration-dependent antimicrobial activity of S200 and S500 samples against *E. coli* B. Figure S5: XRD patterns of the control (a) Fe_2O_3 and (b) Cu_2O NPs.

Author Contributions: Conceptualization, Y.Z. and R.J.M.; methodology, Y.Z., J.E.V., S.L.B., and R.J.M.; software, L.Z.; validation, L.Z., S.L.B., and J.E.V.; formal analysis, L.Z., S.L.B., and A.M.; investigation, L.Z., D.W.P., S.L.B., J.X., J.P., Y.Y., A.M., and J.Y.H.; data curation, L.Z. and S.L.B.; writing—original draft preparation, L.Z.; writing—review and editing, Y.Z. and S.L.B.; supervision, Y.Z., J.E.V., H.H. and Y.-C.H.; project administration, Y.Z.; funding acquisition, Y.Z., J.E.V., and R.J.M. All authors have read and agreed to the published version of the manuscript.

Funding: This project is supported by National Science Foundation (Nos. ECCS-1609815 and ECCS-1808271) for L.Z., D.W.P., Y.Y. and Y.Z., the University of Georgia Research Foundation for R.J.M., and the National Institutes of Health (No. R21AI112768-01A1) for J.E.V.

Acknowledgments: We would like to thank Yoong Sheng Phang to proof-read this manuscript.

Conflicts of Interest: The authors declare no conflict of interest.

References

1. Fauci, A.S. Infectious diseases: Considerations for the 21st century. *Clin. Infect. Dis.* **2001**, *32*, 675–685. [[CrossRef](#)] [[PubMed](#)]
2. World Health Organization. *The World Health Report 2000: Health Systems: Improving Performance*; World Health Organization: Geneva, Switzerland, 2000.
3. Pinner, R.W.; Teutsch, S.M.; Simonsen, L.; Klug, L.A.; Graber, J.M.; Clarke, M.J.; Berkelman, R.L. Trends in infectious diseases mortality in the United States. *Jama* **1996**, *275*, 189–193. [[CrossRef](#)] [[PubMed](#)]
4. Wang, H.; Naghavi, M.; Allen, C.; Barber, R.M.; Bhutta, Z.A.; Carter, A.; Casey, D.C.; Charlson, F.J.; Chen, A.Z.; Coates, M.M. Global, regional, and national life expectancy, all-cause mortality, and cause-specific mortality for 249 causes of death, 1980–2015: A systematic analysis for the Global Burden of Disease Study 2015. *Lancet* **2016**, *388*, 1459–1544. [[CrossRef](#)]
5. Dwyer-Lindgren, L.; Bertozzi-Villa, A.; Stubbs, R.W.; Morozoff, C.; Kutz, M.J.; Huynh, C.; Barber, R.M.; Shackelford, K.A.; Mackenbach, J.P.; Van Lenthe, F.J. US county-level trends in mortality rates for major causes of death, 1980–2014. *Jama* **2016**, *316*, 2385–2401. [[CrossRef](#)]
6. CDC. Outbreak of Listeria Infections Linked to Deli Ham. Available online: <https://www.cdc.gov/listeria/outbreaks/countryham-10-18/index.html> (accessed on 26 May 2020).
7. CDC. Outbreak of Salmonella Infections Linked to Ground Beef. Available online: <https://www.cdc.gov/salmonella/newport-10-18/index.html> (accessed on 26 May 2020).
8. Roca, I.; Akova, M.; Baquero, F.; Carlet, J.; Cavalieri, M.; Coenen, S.; Cohen, J.; Findlay, D.; Gyssens, I.; Heure, O. The global threat of antimicrobial resistance: Science for intervention. *New Microbes New Infect.* **2015**, *6*, 22–29. [[CrossRef](#)]
9. Hajipour, M.J.; Fromm, K.M.; Ashkarran, A.A.; de Aberasturi, D.J.; de Larramendi, I.R.; Rojo, T.; Serpooshan, V.; Parak, W.J.; Mahmoudi, M. Antibacterial properties of nanoparticles. *Trends Biotechnol.* **2012**, *30*, 499–511. [[CrossRef](#)]
10. Hamblin, M.R.; Hasan, T. Photodynamic therapy: A new antimicrobial approach to infectious disease? *Photochem. Photobiol. Sci.* **2004**, *3*, 436–450. [[CrossRef](#)]
11. Furno, F.; Morley, K.S.; Wong, B.; Sharp, B.L.; Arnold, P.L.; Howdle, S.M.; Bayston, R.; Brown, P.D.; Winship, P.D.; Reid, H.J. Silver nanoparticles and polymeric medical devices: A new approach to prevention of infection? *J. Antimicrob. Chemother.* **2004**, *54*, 1019–1024. [[CrossRef](#)]
12. Marambio-Jones, C.; Hoek, E.M. A review of the antibacterial effects of silver nanomaterials and potential implications for human health and the environment. *J. Nanopart. Res.* **2010**, *12*, 1531–1551. [[CrossRef](#)]
13. Hassan, I.A.; Parkin, I.P.; Nair, S.P.; Carmalt, C.J. Antimicrobial activity of copper and copper (I) oxide thin films deposited via aerosol-assisted CVD. *J. Mater. Chem. B* **2014**, *2*, 2855–2860. [[CrossRef](#)]
14. Zhu, L.; Basnet, P.; Larson, S.R.; Jones, L.P.; Howe, J.Y.; Tripp, R.A.; Zhao, Y. Visible Light-Induced Photoelectrochemical and Antimicrobial Properties of Hierarchical CuBi₂O₄ by Facile Hydrothermal Synthesis. *ChemistrySelect* **2016**, *1*, 1518–1524. [[CrossRef](#)]
15. Mezziani, M.J.; Dong, X.; Zhu, L.; Jones, L.P.; LeCroy, G.E.; Yang, F.; Wang, S.; Wang, P.; Zhao, Y.; Yang, L. Visible-light-activated bactericidal functions of carbon “Quantum” dots. *ACS Appl. Mater. Interfaces* **2016**, *8*, 10761–10766. [[CrossRef](#)] [[PubMed](#)]
16. Abo-Zeid, Y.; Williams, G.R. The potential anti-infective applications of metal oxide nanoparticles: A systematic review. *Wiley Interdiscip. Rev. Nanomed. Nanobiotechnol.* **2020**, *12*, e1592. [[CrossRef](#)] [[PubMed](#)]
17. Baptista, P.V.; McCusker, M.P.; Carvalho, A.; Ferreira, D.A.; Mohan, N.M.; Martins, M.; Fernandes, A.R. Nano-Strategies to Fight Multidrug Resistant Bacteria—“A Battle of the Titans”. *Front. Microbiol.* **2018**, *9*, 1441. [[CrossRef](#)]
18. Wang, W.; Huang, G.; Yu, J.C.; Wong, P.K. Advances in photocatalytic disinfection of bacteria: Development of photocatalysts and mechanisms. *J. Environ. Sci.* **2015**, *34*, 232–247. [[CrossRef](#)]
19. Nararom, M.; Thepa, S.; Kongkiattikajorn, J.; Songprakorp, R. Disinfection of water containing Escherichia coli by use of a compound parabolic concentrator: Effect of global solar radiation and reactor surface treatment. *Res. Chem. Intermed.* **2015**, *41*, 6543–6558. [[CrossRef](#)]
20. Marugan, J.; van Grieken, R.; Pablos, C.; Lucila Satuf, M.; Cassano, A.E.; Alfano, O.M. Photocatalytic inactivation of Escherichia coli aqueous suspensions in a fixed-bed reactor. *Catal. Today* **2015**, *252*, 143–149. [[CrossRef](#)]

21. Markowska-Szczupak, A.; Ulfig, K.; Morawski, A.W. The application of titanium dioxide for deactivation of bioparticulates: An overview. *Catal. Today* **2011**, *169*, 249–257. [[CrossRef](#)]
22. Liou, J.-W.; Chang, H.-H. Bactericidal Effects and Mechanisms of Visible Light-Responsive Titanium Dioxide Photocatalysts on Pathogenic Bacteria. *Arch. Immunol. Et Ther. Exp.* **2012**, *60*, 267–275. [[CrossRef](#)]
23. Li, Q.; Mahendra, S.; Lyon, D.Y.; Brunet, L.; Liga, M.V.; Li, D.; Alvarez, P.J.J. Antimicrobial nanomaterials for water disinfection and microbial control: Potential applications and implications. *Water Res.* **2008**, *42*, 4591–4602. [[CrossRef](#)]
24. Janpetch, N.; Vanichvattanadecha, C.; Rujiravanit, R. Photocatalytic disinfection of water by bacterial cellulose/N-F co-doped TiO₂ under fluorescent light. *Cellulose* **2015**, *22*, 3321–3335. [[CrossRef](#)]
25. Bogdan, J.; Zarzynska, J.; Plawinska-Czarnak, J. Comparison of Infectious Agents Susceptibility to Photocatalytic Effects of Nanosized Titanium and Zinc Oxides: A Practical Approach. *Nanoscale Res. Lett.* **2015**, *10*. [[CrossRef](#)] [[PubMed](#)]
26. Amin, M.T.; Alazba, A.A. A review of nanomaterials based membranes for removal of contaminants from polluted waters. *Membr. Water Treat.* **2014**, *5*, 123–146. [[CrossRef](#)]
27. Hossain, F.; Perales-Perez, O.J.; Hwang, S.; Roman, F. Antimicrobial nanomaterials as water disinfectant: Applications, limitations and future perspectives. *Sci. Total Environ.* **2014**, *466*, 1047–1059. [[CrossRef](#)] [[PubMed](#)]
28. Basnet, P.; Larsen, G.K.; Jadeja, R.P.; Hung, Y.-C.; Zhao, Y. α -Fe₂O₃ Nanocolumns and Nanorods Fabricated by Electron Beam Evaporation for Visible Light Photocatalytic and Antimicrobial Applications. *ACS Appl. Mater. Interfaces* **2013**, *5*, 2085–2095. [[CrossRef](#)]
29. Ocoy, I.; Paret, M.L.; Ocoy, M.A.; Kunwar, S.; Chen, T.; You, M.; Tan, W. Nanotechnology in Plant Disease Management: DNA-Directed Silver Nanoparticles on Graphene Oxide as an Antibacterial against *Xanthomonas perforans*. *ACS Nano* **2013**, *7*, 8972–8980. [[CrossRef](#)]
30. Ocoy, I.; Temiz, M.; Celik, C.; Altinsoy, B.; Yilmaz, V.; Duman, F. A green approach for formation of silver nanoparticles on magnetic graphene oxide and highly effective antimicrobial activity and reusability. *J. Mol. Liq.* **2017**, *227*, 147–152. [[CrossRef](#)]
31. Baldemir, A.; Köse, N.B.; Ildiz, N.; İlğün, S.; Yusufbeyoğlu, S.; Yilmaz, V.; Ocoy, I. Synthesis and characterization of green tea (*Camellia sinensis* (L.) Kuntze) extract and its major components-based nanoflowers: A new strategy to enhance antimicrobial activity. *RSC Adv.* **2017**, *7*, 44303–44308. [[CrossRef](#)]
32. Celik, C.; Ildiz, N.; Ocoy, I. Building block and rapid synthesis of catecholamines-inorganic nanoflowers with their peroxidase-mimicking and antimicrobial activities. *Sci. Rep.* **2020**, *10*, 2903. [[CrossRef](#)]
33. Jung, W.K.; Koo, H.C.; Kim, K.W.; Shin, S.; Kim, S.H.; Park, Y.H. Antibacterial activity and mechanism of action of the silver ion in *Staphylococcus aureus* and *Escherichia coli*. *Appl. Environ. Microbiol.* **2008**, *74*, 2171–2178. [[CrossRef](#)]
34. Ren, J.; Wang, W.; Sun, S.; Zhang, L.; Wang, L.; Chang, J. Crystallography facet-dependent antibacterial activity: The case of Cu₂O. *Ind. Eng. Chem. Res.* **2011**, *50*, 10366–10369. [[CrossRef](#)]
35. Applerot, G.; Lellouche, J.; Lipovsky, A.; Nitzan, Y.; Lubart, R.; Gedanken, A.; Banin, E. Understanding the antibacterial mechanism of CuO nanoparticles: Revealing the route of induced oxidative stress. *Small* **2012**, *8*, 3326–3337. [[CrossRef](#)] [[PubMed](#)]
36. Beer, C.; Foldbjerg, R.; Hayashi, Y.; Sutherland, D.S.; Autrup, H. Toxicity of silver nanoparticles—Nanoparticle or silver ion? *Toxicol. Lett.* **2012**, *208*, 286–292. [[CrossRef](#)] [[PubMed](#)]
37. Bao, H.; Yu, X.; Xu, C.; Li, X.; Li, Z.; Wei, D.; Liu, Y. New Toxicity Mechanism of Silver Nanoparticles: Promoting Apoptosis and Inhibiting Proliferation. *PLoS ONE* **2015**, *10*, e0122535. [[CrossRef](#)] [[PubMed](#)]
38. Munro, C.J.; Nguyen, M.A.; Falgons, C.; Chaudhry, S.; Olagunju, M.O.; Bode, A.; Bobé, C.; Portela, M.E.; Knecht, M.R.; Collins, K.M. Identification of toxicity effects of Cu₂O materials on *C. elegans* as a function of environmental ionic composition. *Environ. Sci. Nano* **2020**, *7*, 645–655. [[CrossRef](#)] [[PubMed](#)]
39. Ahamed, M.; Siddiqui, M.A.; Akhtar, M.J.; Ahmad, I.; Pant, A.B.; Alhadlaq, H.A. Genotoxic potential of copper oxide nanoparticles in human lung epithelial cells. *Biochem. Biophys. Res. Commun.* **2010**, *396*, 578–583. [[CrossRef](#)] [[PubMed](#)]
40. De Jong, W.H.; De Rijk, E.; Bonetto, A.; Wohlleben, W.; Stone, V.; Brunelli, A.; Badetti, E.; Marcomini, A.; Gosens, I.; Cassee, F.R. Toxicity of copper oxide and basic copper carbonate nanoparticles after short-term oral exposure in rats. *Nanotoxicology* **2019**, *13*, 50–72. [[CrossRef](#)]

41. Pegalajar-Jurado, A.; Wold, K.A.; Joslin, J.M.; Neufeld, B.H.; Arabea, K.A.; Suazo, L.A.; McDaniel, S.L.; Bowen, R.A.; Reynolds, M.M. Reprint of: Nitric oxide-releasing polysaccharide derivative exhibits 8-log reduction against *Escherichia coli*, *Acinetobacter baumannii* and *Staphylococcus aureus*. *J. Control. Release* **2015**, *220*, 617–623. [[CrossRef](#)]
42. Jin, T.; Sun, D.; Su, J.; Zhang, H.; Sue, H.J. Antimicrobial efficacy of zinc oxide quantum dots against *Listeria monocytogenes*, *Salmonella enteritidis*, and *Escherichia coli* O157: H7. *J. Food Sci.* **2009**, *74*, M46–M52. [[CrossRef](#)]
43. Esteban-Cubillo, A.; Pecharromán, C.; Aguilar, E.; Santarén, J.; Moya, J.S. Antibacterial activity of copper monodispersed nanoparticles into sepiolite. *J. Mater. Sci.* **2006**, *41*, 5208–5212. [[CrossRef](#)]
44. Baranwal, A.; Srivastava, A.; Kumar, P.; Bajpai, V.K.; Maurya, P.K.; Chandra, P. Prospects of Nanostructure Materials and Their Composites as Antimicrobial Agents. *Front. Microbiol.* **2018**, *9*, 422. [[CrossRef](#)]
45. Tran, C.D.; Makuvaza, J.; Munson, E.; Bennett, B. Biocompatible Copper Oxide Nanoparticle Composites from Cellulose and Chitosan: Facile Synthesis, Unique Structure, and Antimicrobial Activity. *ACS Appl. Mater. Interfaces* **2017**, *9*, 42503–42515. [[CrossRef](#)]
46. Macomber, L.; Imlay, J.A. The iron-sulfur clusters of dehydratases are primary intracellular targets of copper toxicity. *Proc. Natl. Acad. Sci. USA* **2009**, *106*, 8344–8349. [[CrossRef](#)]
47. Qiu, X.; Liu, M.; Sunada, K.; Miyauchi, M.; Hashimoto, K. A facile one-step hydrothermal synthesis of rhombohedral CuFeO_2 crystals with antiviral property. *Chem. Commun.* **2012**, *48*, 7365–7367. [[CrossRef](#)]
48. Abdelhamid, H.N.; Kumaran, S.; Wu, H.-F. One-pot synthesis of CuFeO_2 nanoparticles capped with glycerol and proteomic analysis of their nanocytotoxicity against fungi. *RSC Adv.* **2016**, *6*, 97629–97635. [[CrossRef](#)]
49. Köferstein, R. Synthesis, phase evolution and properties of phase-pure nanocrystalline BiFeO_3 prepared by a starch-based combustion method. *J. Alloys Compd.* **2014**, *590*, 324–330. [[CrossRef](#)]
50. Rodríguez-Carvajal, J. Recent advances in magnetic structure determination by neutron powder diffraction. *Phys. B Condens. Matter* **1993**, *192*, 55–69. [[CrossRef](#)]
51. Mahieux, P.Y.; Aubert, J.E.; Cyr, M.; Coutand, M.; Husson, B. Quantitative mineralogical composition of complex mineral wastes—contribution of the Rietveld method. *Waste Manag.* **2010**, *30*, 378–388. [[CrossRef](#)]
52. Leon-Reina, L.; Garcia-Mate, M.; Alvarez-Pinazo, G.; Santacruz, I.; Vallcorba, O.; De la Torre, A.G.; Aranda, M.A. Accuracy in Rietveld quantitative phase analysis: A comparative study of strictly monochromatic Mo and Cu radiations. *J. Appl. Crystallogr.* **2016**, *49*, 722–735. [[CrossRef](#)]
53. Shanmugam, C.; Sivasubramanian, G.; Parthasarathi, B.; Baskaran, K.; Balachander, R.; Parameswaran, V.R. Antimicrobial, free radical scavenging activities and catalytic oxidation of benzyl alcohol by nano-silver synthesized from the leaf extract of *Aristolochia indica* L.: A promenade towards sustainability. *Appl. Nanosci.* **2016**, *6*, 711–723. [[CrossRef](#)]
54. Islam, S.M.; Roy, A.S.; Mondal, P.; Mubarak, M.; Mondal, S.; Hossain, D.; Banerjee, S.; Santra, S.C. Synthesis, catalytic oxidation and antimicrobial activity of copper(II) Schiff base complex. *J. Mol. Catal. A Chem.* **2011**, *336*, 106–114. [[CrossRef](#)]
55. Edison, T.J.I.; Sethuraman, M. Instant green synthesis of silver nanoparticles using *Terminalia chebula* fruit extract and evaluation of their catalytic activity on reduction of methylene blue. *Process Biochem.* **2012**, *47*, 1351–1357. [[CrossRef](#)]
56. Brown, G.T.; Darwent, J.R. Methyl orange as a probe for photooxidation reactions of colloidal titanium dioxide. *J. Phys. Chem.* **1984**, *88*, 4955–4959. [[CrossRef](#)]
57. Giannousi, K.; Lafazanis, K.; Arvanitidis, J.; Pantazaki, A.; Dendrinou-Samara, C. Hydrothermal synthesis of copper based nanoparticles: Antimicrobial screening and interaction with DNA. *J. Inorg. Biochem.* **2014**, *133*, 24–32. [[CrossRef](#)]
58. Meghana, S.; Kabra, P.; Chakraborty, S.; Padmavathy, N. Understanding the pathway of antibacterial activity of copper oxide nanoparticles. *RSC Adv.* **2015**, *5*, 12293–12299. [[CrossRef](#)]
59. Antonoglou, O.; Lafazanis, K.; Mourdikoudis, S.; Vourlias, G.; Lialiaris, T.; Pantazaki, A.; Dendrinou-Samara, C. Biological relevance of CuFeO_2 nanoparticles: Antibacterial and anti-inflammatory activity, genotoxicity, DNA and protein interactions. *Mater. Sci. Eng. C* **2019**, *99*, 264–274. [[CrossRef](#)]
60. Bai, H.; Liu, Z.; Sun, D.D. Hierarchical ZnO/Cu “corn-like” materials with high photodegradation and antibacterial capability under visible light. *Phys. Chem. Chem. Phys.* **2011**, *13*, 6205–6210. [[CrossRef](#)]
61. Bondarenko, O.; Ivask, A.; Käkinen, A.; Kahru, A. Sub-toxic effects of CuO nanoparticles on bacteria: Kinetics, role of Cu ions and possible mechanisms of action. *Environ. Pollut.* **2012**, *169*, 81–89. [[CrossRef](#)]

62. Fan, W.; Wang, X.; Cui, M.; Zhang, D.; Zhang, Y.; Yu, T.; Guo, L. Differential oxidative stress of octahedral and cubic Cu₂O micro/nanocrystals to *Daphnia magna*. *Environ. Sci. Technol.* **2012**, *46*, 10255–10262. [[CrossRef](#)]
63. Von Moos, N.; Slaveykova, V.I. Oxidative stress induced by inorganic nanoparticles in bacteria and aquatic microalgae—state of the art and knowledge gaps. *Nanotoxicology* **2014**, *8*, 605–630. [[CrossRef](#)]
64. Wu, P.; Imlay, J.A.; Shang, J.K. Mechanism of *Escherichia coli* inactivation on palladium-modified nitrogen-doped titanium dioxide. *Biomaterials* **2010**, *31*, 7526–7533. [[CrossRef](#)]
65. Imlay, J.A. The molecular mechanisms and physiological consequences of oxidative stress: Lessons from a model bacterium. *Nat. Rev. Microbiol.* **2013**, *11*, 443–454. [[CrossRef](#)]
66. Midander, K.; Cronholm, P.; Karlsson, H.L.; Elihn, K.; Möller, L.; Leygraf, C.; Wallinder, I.O. Surface characteristics, copper release, and toxicity of nano- and micrometer-sized copper and copper (II) oxide particles: A cross-disciplinary study. *Small* **2009**, *5*, 389–399. [[CrossRef](#)]
67. Pendleton, J.N.; Gorman, S.P.; Gilmore, B.F. Clinical relevance of the ESKAPE pathogens. *Expert Rev. Anti-Infect. Ther.* **2013**, *11*, 297–308. [[CrossRef](#)]
68. Magill, S.S.; Edwards, J.R.; Bamberg, W.; Beldavs, Z.G.; Dumyati, G.; Kainer, M.A.; Lynfield, R.; Maloney, M.; McAllister-Hollod, L.; Nadle, J.; et al. Multistate Point-Prevalence Survey of Health Care-Associated Infections. *N. Engl. J. Med.* **2014**, *370*, 1198–1208. [[CrossRef](#)]

Publisher's Note: MDPI stays neutral with regard to jurisdictional claims in published maps and institutional affiliations.



© 2020 by the authors. Licensee MDPI, Basel, Switzerland. This article is an open access article distributed under the terms and conditions of the Creative Commons Attribution (CC BY) license (<http://creativecommons.org/licenses/by/4.0/>).